Dalton Transactions

ROYAL SOCIETY OF CHEMISTRY

PAPER

View Article Online
View Journal | View Issue

Check for updates

Cite this: *Dalton Trans.*, 2024, **53**, 4652

Terpyridine isomerism as a tool for tuning red-to-NIR emissive properties in heteronuclear gold(I)–thallium(I) complexes†

David Royo,[a] Sonia Moreno,[a] María Rodríguez-Castillo,[a] Miguel Monge,[a] M. Elena Olmos,*[a] Fedor I. Zubkov,[b] Anastasia A. Pronina,[b] Ghodrat Mahmoudi*[c,d] and José M. López-de-Luzuriaga*[a]

Received 12th December 2023,
Accepted 2nd February 2024

DOI: 10.1039/d3dt04161a

rsc.li/dalton

The polymeric linear chain $[AuTl(C_6Cl_5)_2]_n$ reacts with three terpyridine-type ligands substituted with thiophene groups containing N-donor centres in different relative positions (**L$_1$**, **L$_2$** and **L$_3$**), leading to the Au(I)/Tl(I) complexes $[AuTl(C_6Cl_5)_2(\mathbf{L_1})]_n$ (**1**), $[\{AuTl(C_6Cl_5)_2\}_2(\mathbf{L_2})]_n$ (**2**) and $[AuTl(C_6Cl_5)_2(\mathbf{L_3})]_n$ (**3**). X-Ray diffraction studies reveal that **L$_1$** acts as a chelate, while **L$_2$** and **L$_3$** act as bridging ligands, resulting in different coordination indexes for the thallium(I) centre. These structural differences strongly influence their optical properties, and while compounds **2** and **3** emit near the limit of the visible range, complex **1** emits in the infrared region. DFT calculations have also been carried out in order to determine the origin of the electronic transitions responsible for their optical properties.

Introduction

For many years, intermolecular non-covalent interactions have been the origin of novel supramolecular entities with amazing architectures and properties. They appear between metal atoms or between non-metal atoms of different ligands and metal centres. Among them, those observed in gold derivatives are particularly frequent in coordination and organometallic complexes, which gave rise to a definite term: *aurophilicity*.[1] As a result of the subsequent research on heteronuclear derivatives of gold, this term soon evolved to a more general one, *metallophilicity*,[2] because of the increasing number of examples of heterometallic gold-containing compounds showing gold and closed-shell heterometallic centres located at distances shorter than the sum of their van der Waals radii in the solid state. These interactions have been the object of study in several laboratories both from experimental and theoretical viewpoints for many years because, in addition to their influence on the solid-state structures, they are also associated with intriguing physical and chemical properties.[3] In-depth studies of the properties of complexes bearing these interactions have been performed including their luminescence properties, and the computational studies carried out on models of these complexes have demonstrated that their origin can be found in the type and strength of the metallophillic interactions, as well as in the environment of the metal centres. Thus, for instance, luminescence has been found in complexes displaying interactions between Au(I) and other metal ions such as Ag(I),[4] Cu(I),[5] Pb(II)[6] or Tl(I).[7] Thanks to thorough structural and computational studies, it now seems clear that the ligands do not have a passive role in the optical behavior of the metal complexes that contain them; in contrast, they influence very important aspects, like the electron density on the metal centres, leading them to act as Lewis acids or bases, or their hardness or softness, which favours rigid or flexible structures. In summary, the combination of metal interactions and ligands gives rise to an almost infinite source of possibilities that leads in turn, among others, to a great variety of photoluminescence properties.

Regarding the strategies for synthesizing complexes exhibiting heterometallic interactions, our laboratory is a pioneer in very successfully using the acid–base strategy, that is, reactions in which a basic precursor (typically bis(perhalophenyl)aurate(I) complexes) reacts with a Lewis acid salt in the presence of ligands of different typologies and with different donor

[a]*Departamento de Química, Instituto de Investigación en Química (IQUR), Complejo Científico Tecnológico, Madre de Dios 53, Universidad de La Rioja, 26006 Logroño, Spain. E-mail: m-elena.olmos@unirioja.es, josemaria.lopez@unirioja.es*
[b]*Department of Organic Chemistry, RUDN University, 6 Miklukho-Maklaya St, Moscow, 117198, Russia*
[c]*Department of Chemistry, Faculty of Science, University of Maragheh, P.O. Box 55136-83111, Maragheh, Iran. E-mail: ghodratmahmoudi@gmail.com*
[d]*Samara State Technical University, Molodogvardeyskaya Str 244, Samara 443100, Russia*

†Electronic supplementary information (ESI) available: Spectroscopic characterization, structural characterization and computational studies. CCDC 2305451–2305453. For ESI and crystallographic data in CIF or other electronic format see DOI: https://doi.org/10.1039/d3dt04161a

centres. Depending on the metals involved and the type of ligands (number and nature of donor centres), we were able to obtain different geometries and nuclearities, from single molecules[8] to linear,[9] two- or three-dimensional[10] architectures, each one displaying different optical properties associated with their particular characteristics.

In the particular case of gold(I)–thallium(I) derivatives, our contributions include discrete molecules,[11] polymeric chains,[12] as well as two- and three-dimensional[13] networks containing mono- or bi-dentate O- or N-donor ligands, or even taking advantage of the donor abilities of the neighbour halogens that may interact with metals,[14] thus favouring the formation of supramolecular structures of a higher dimension. We have also tested some cyclic polydentate ligands containing different numbers of O-, S- and/or N-donor atoms,[15] although, in these cases, their cyclic nature and the high number of donor centres that saturate the thallium environment restrict their structural possibilities of growing from discrete molecules or one-dimensional chains to higher dimensionality entities.

In order to increase our knowledge about this kind of system that allows us to carry out a rational synthesis of complexes with predefined properties, we aim to explore the use of other polydentate ligands with geometries that could lead to novel frameworks and that may give rise to original structures and influence their optical properties. For example, we focused on the use of polydentate ligands in which the relative position of their donor atoms facilitates different connections between the metals. Thus, in this paper, we explore the structural possibilities of three terpyridine-type ligands substituted with thiophene groups with the N-donor centres in different relative positions, *ortho*, *meta* or *para*, in order to analyse their influence on the geometries of the final products, as well as the effect that the structures of these new complexes have on their photophysical properties.

Results and discussion

Synthesis and characterization of the complexes

By the reaction of equimolecular amounts of the polymeric linear chain $[AuTl(C_6Cl_5)_2]_n$ [16] with the terpyridine derivatives 4′-(thiophene-2-yl)-2,2′:6′,2″-terpyridine (**L$_1$**), 4′-(thiophene-2-yl)-3,2′:6′,3″-terpyridine (**L$_2$**) or 4′-(thiophene-2-yl)-4,2′:6′,4″-terpyridine (**L$_3$**) in dry tetrahydrofuran, the complexes $[AuTl(C_6Cl_5)_2(\mathbf{L_1})]_n$ (**1**), $[\{AuTl(C_6Cl_5)_2\}_2(\mathbf{L_2})]_n$ (**2**) or $[AuTl(C_6Cl_5)_2(\mathbf{L_3})]_n$ (**3**) were obtained in good yields (see the Experimental section). Considering that the stoichiometry in **2** is not the expected one for the molar ratio of the reagents employed and that it differs from that of complexes **1** and **3** (see Scheme 1), the same reactions were carried out varying the molar ratios of $[AuTl(C_6Cl_5)_2]_n$ and **L$_1$**, **L$_2$** or **L$_3$** to 1 : 2 and 2 : 1. Nevertheless, whatever the molar ratio employed, the resulting product is always the same, **1**, **2** or **3**, in all the cases.

The IR spectra of the three complexes display the expected vibrations due to the C=N and C=C bonds of the ligands at

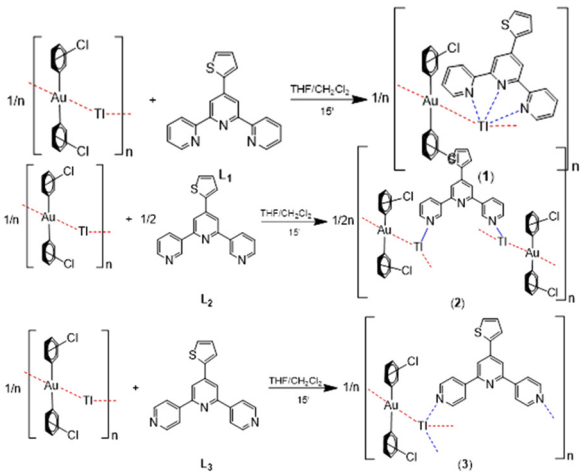

Scheme 1 Synthesis of complexes **1–3**.

1600 cm^{-1} and within the range 1480–1423 cm^{-1}, respectively. They all also show the absorptions due to the pentachlorophenyl groups bonded to gold(I) at 838–823 and 616–613 cm^{-1}.[17]

In the ^{1}H NMR spectra of complexes **1–3** all the resonances due to the protons of the terpyridine and thiophene groups appear slightly shifted to each other due to the different relative positions of the nitrogen centres, and all of them are also shifted relative to those of the free ligands (see the ESI†), suggesting that these ligands remain coordinated to the thallium centres in solution.

Interestingly, the molar conductivity measurements of the three complexes in methanol afforded values typical of 1 : 1 electrolytes. These data, together with those of the ^{1}H NMR spectra, suggest that the three complexes are dissociated into their ionic counterparts $[Tl(\mathbf{L})]^+$ and $[Au(C_6Cl_5)_2]^-$ in solution.

Finally, the MALDI(−) mass spectra of the three complexes display the peak corresponding to the $[Au(C_6Cl_5)_2]^-$ fragment at m/z = 694 as the base peak, while in their MALDI(+) mass spectra the base peak corresponds to the fragment $[Tl(\mathbf{L_1})]^+$ in the case of complex **1** (m/z = 519) or $[Tl(DCTB)]^+$ and $[Tl(DCTB)_2]^+$ in the cases of **2** and **3**, which are located at m/z = 455 or 705, respectively (see the Experimental section; DCTB corresponds to *trans*-2-[3-(4-*tert*-butylphenyl)-2-methyl-2-propenylidene]-malononitrile used as a matrix in MALDI experiments).

X-ray diffraction studies

The crystal structures of complexes **1–3** were established by X-ray diffraction studies on single crystals grown by slow diffusion of *n*-hexane into a saturated solution of the complex in tetrahydrofuran (**1**) or acetone (**2** and **3**).

All of them feature polymeric chains of alternating bis(pentachloropheny)aurate(I) anions and thallium(I) centres bonded to the polydentate N-donor ligands, which are linked through unsupported Au···Tl interactions with distances of 2.9352(18) Å in **2** and 3.1598(5) Å in **3** (see Fig. 1–3 and Table 1). These values are similar to most of the Au–Tl distances found in

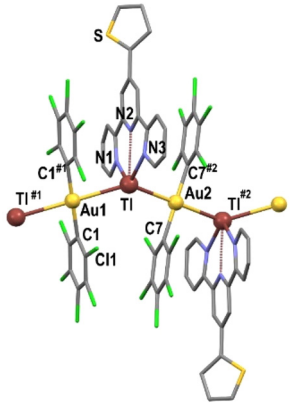

Fig. 1 Partial view of the polymeric chain in the crystal structure of **1** formed *via* Au···Tl interactions with the labelling scheme for the atom positions. Hydrogen atoms have been omitted for clarity. #1: $-x + 1, -y + 1, -z + 1$; #2: $-x + 1, -y, -z + 1$.

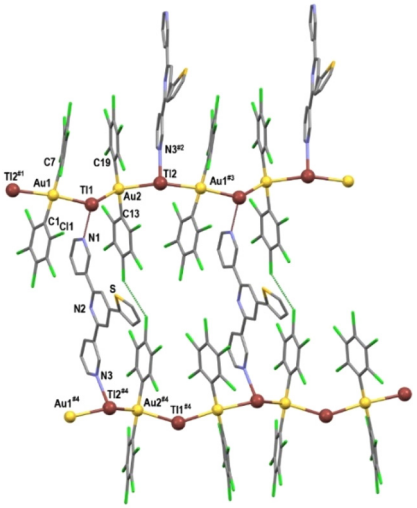

Fig. 2 Partial view of the 2D network in the crystal structure of **2** formed *via* Au···Tl interactions and bridging L_2 ligands with the labelling scheme for the atom positions. Hydrogen atoms have been omitted for clarity. #1: $x, y + 1, z$; #2: $x, -y, z - 1/2$; #3: $x, y - 1, z$; #4: $x, -y, z + 1/2$.

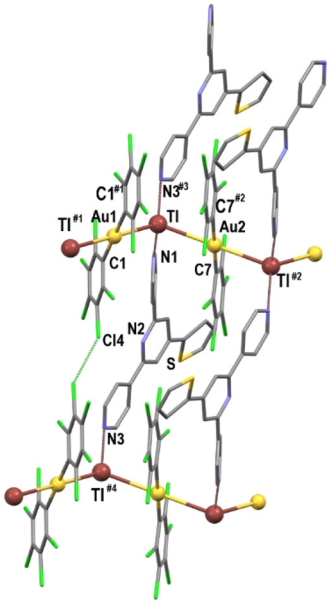

Fig. 3 Partial view of the 2D network in the crystal structure of **3** formed *via* Au···Tl interactions and bridging L_3 ligands with the labelling scheme for the atom positions. Hydrogen atoms have been omitted for clarity. #1: $-x + 2, -y, -z$; #2: $-x + 1, -y, -z$; #3: $x, y, z - 1$; #4: $-x + 2, -y, -z + 1$.

other polynuclear Au/Tl systems formed *via* unsupported metal–metal interactions and containing aromatic N-donor ligands at thallium, which vary from 2.9647(2) to 3.4899(6) Å.[10,13,15h,18]

The gold atoms, which in **1** and **3** lie in inversion centres, are linearly coordinated to two C_6Cl_5 ligands with Au–C bond lengths between 2.042(14) Å in **2** and 2.120(8) Å in **1**, while the thallium(I) centres bind the neutral N-donor ligands, which are the responsible for the differences found in the three crystal structures due to the relative positions of the nitrogen atoms in the aromatic rings of $\mathbf{L_1}$–$\mathbf{L_3}$.

Thus, the disposition of the nitrogen atoms in $\mathbf{L_1}$ favours its behaviour as a chelate ligand, and, therefore, in **1** it is coordinated to Tl(I) through its three donor atoms, although with asymmetric Tl–N distances of 2.676(11), 2.726(10) and 2.850(9) Å, the longest one corresponding to the one of the central pyridyl ring, which can be considered as only interacting with (instead of being bonded to) thallium. This last Tl–N distance compares well with those in $[Au_2Tl_2(C_6Cl_5)_4(bipy)]\cdot(acacH)$ (2.874(5) Å)[18c] and $[AuTl(C_6Cl_5)_2(bipy)_{0.5}]_n$ (2.839(8) Å),[13] while the former ones lie within the range of Tl–N bond distances found in related Au/Tl complexes containing 2,2′-bipyridine, 4,4′-bipyridine or 1,10-phenanthroline as the ligand (Tl–N distances ranging from 2.641(9) to 2.785(3) Å).[10,13,18a] This leads to the formation of a polymeric one-dimensional array that runs parallel to the crystallographic *y* axis, as shown in Fig. 1 and Fig. S10 in the ESI.†

In contrast, in the crystal structures of **2** and **3**, the *ortho* and *para* relative positions of the nitrogen atoms in the functionalized terpyridine ligands $\mathbf{L_2}$ and $\mathbf{L_3}$ lead to their coordination to thallium as bridging instead of chelating ligands, which connect adjacent polymetallic chains, thus affording two-dimensional networks (Fig. 2 and 3, and Fig. S11 and S12 in ESI†). In both cases, the nitrogen atom of the central ring in each neutral ligand remains uncoordinated, while the other two bind the thallium atoms with dissimilar Tl–N distances of 2.621(14) and 2.703(14) Å in **2** and of 2.724(4) and 2.826(5) Å in **3**, the first one being the shortest found in related Au/Tl derivatives containing aromatic N-donor ligands bonded to thallium.[10,13,15h,18] The connection of the polymetallic chains through the neutral ligands is additionally reinforced by the presence of Cl···Cl contacts, of 3.484(6) Å in **2** and 3.319(4) Å in **3**, between halogen atoms of neighbouring chains, as shown in Fig. 2 and 3. Similar halogen···halogen contacts have

Table 1 Main bond or contact distances (Å) and angles (°) in the crystal structures of **1–3**

	Au···Tl	Au–C	Tl–N	Cl···Cl	Tl–Au–Tl	Au–Tl–Au	C–Au–C	N–Tl–N	N–Tl–Au
1	3.0779(5) 2.9834(5)	2.120(8) 2.086(11)	2.676(11) 2.726(10) 2.850(9)	—	180.00(2)	128.44(17)	180.0	116.1(3) 59.6(3) 56.5(3)	78.8(2)–122.9(2)
2	2.9352(18) 2.9392(9) 2.9993(9) 3.0084(18)	2.042(14) 2.054(13) 2.058(13) 2.084(13)	2.621(14) 2.703(14)	3.484(6)	173.03(4) 118.20(4)	137.13(6) 145.16(4)	178.3(6) 177.4(6)	—	98.8(3) 99.2(3)
3	3.0847(4) 3.1598(5)	2.065(4) 2.059(4)	2.724(4) 2.826(5)	3.319(4)	180.0	128.25(16)	180.0	97.34(15)	82.08(8)–124.19(11)

been observed in other bis(perhalophenyl)aurate(I)-containing complexes.[4a,9]

The differences observed in the behaviour of $\mathbf{L_1}$, $\mathbf{L_2}$ and $\mathbf{L_3}$ as chelating (**1**) or bridging ligands, as well as in the stoichiometries in **2** and **3**, which lead to the presence of one or two bridging terpy ligands, respectively, result in different coordination numbers of 5 (**1**), 3 (**2**) and 4 (**3**) for the thallium(I) centres (see Fig. 4). Nevertheless, no obvious coordination environment can be clearly assigned to them, although in all of them the thallium(I) lone pair seems to be stereochemically active, and the widest angle around Tl(I) corresponds to the Au–TlAu, which exhibits values of 128.44(17)° (**1**), 137.13(6) and 145.16(4)° (**2**), and 128.25(16)° (**3**).

Optical properties of the complexes

As expected, the three complexes display a rich optical behaviour. In this case, the differences in the positions of the nitrogen donor centres in the terpyridines and their bonding mode, as we have commented, lead to different structural dispositions and, at the same time, very interestingly, give rise to different optical responses when the derivatives are exposed to UV-Vis light. Also, they show big differences in the energies of the emissions if they are compared with other gold(I)–thallium (I) complexes with different ligands, having the same or different types of donor centres, reported in previous contributions from our group.[18] Obviously, as it will be shown in these examples, terpyridine type ligands lead to red-shifted emissions.

Thus, firstly, the analyses of the UV-Vis spectra and the luminescence studies of the three complexes in tetrahydrofuran solutions are likely to confirm our previous comments about the dissociative processes in counterions that could take place in solution. The spectra of the three derivatives are very similar to each other (see the ESI†). Although the presence of the absorptions of $NBu_4[Au(C_6Cl_5)_2]$ below the main profile spectrum can be inferred, the spectra basically recall those of the terpy ligands instead of a combination of $\mathbf{L_1}$–$\mathbf{L_3}$ and $NBu_4[Au(C_6Cl_5)_2]$, especially for compounds **2** and **3**, showing non-significant shifts that can arise from the interactions between the metal centres and ligands and/or solvent molecules. In addition, although the structures in the solid state show supramolecular entities, no additional bands appear at lower energies, bands that usually have their origins in orbitals that appear as a consequence of the intermetallic interactions. Similarly, the three complexes do not show luminescence in solution either, suggesting that the absence of these intermetallic interactions in solution is a fact to take into consideration in the generation of excited states responsible for the emissions.

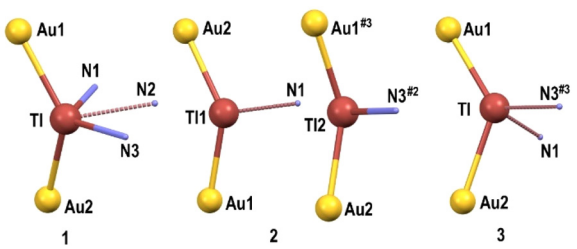

Fig. 4 Coordination environments for the thallium(I) atoms in the crystal structures of complexes **1–3**.

Thus, by contrast, the diffuse reflectance spectra in the solid state are quite different from those of the precursors. In all cases the absorption band edges shift to much lower energies than those of the precursors, reaching more than 700 nm for **1**, 625 nm for **2**, or 550 nm for **3**, respectively. Alternatively, the more energetic part of the spectra match those of the precursors in all cases, with maxima at 273 and 330 nm in the three cases, showing additional maxima at 445 and 600 nm for **1**, 423 and 520 nm for **2**, and 400 nm for **3** (see Fig. 5). They appear close in energies to those obtained in solution; therefore, considering the previous features, these bands are likely to arise from internal $\pi \rightarrow \pi^*$ transitions in the pentachlorophenyl or terpyridine ligands and/or charge transfer transitions involving gold(I) and the perhalophenyl rings. By contrast, the less energetic transitions are likely to be related to transitions in which the metals are involved to some extent, such as in charge transfer transitions with the ligands and/or between them because of the intermetallic interactions. These assumptions were further confirmed thanks to the computational studies carried out on models of these complexes (see the Computational section).

The three complexes show intense low energy emissions at room temperature and at 77 K in the solid state (see Fig. 6). Thus, complexes **1–3** emit at 966 nm (exc. at 694 nm), 660 nm

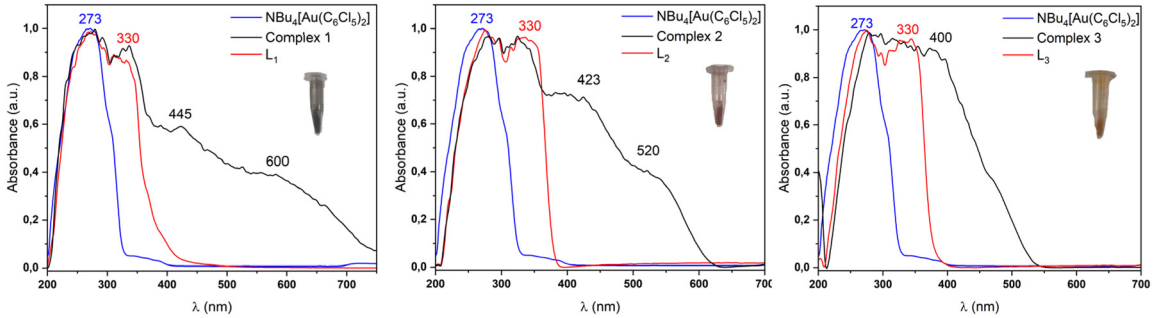

Fig. 5 Experimental UV-Vis solid state absorption spectra for complexes **1–3** (black), ligand (red) and gold precursor (blue).

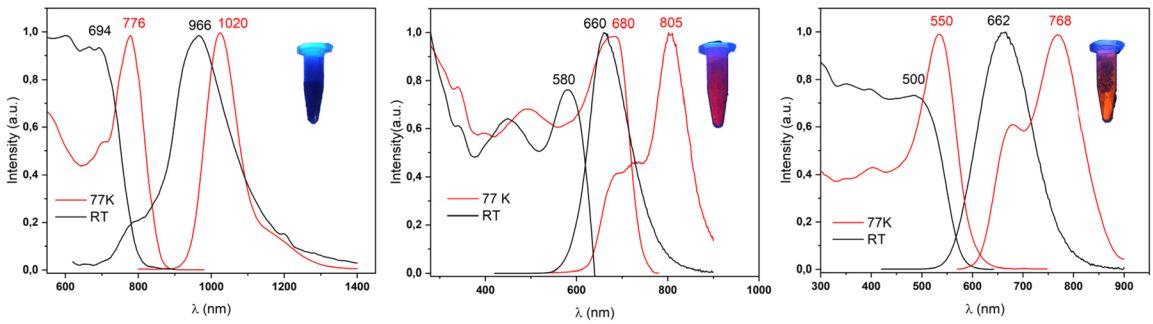

Fig. 6 Excitation and emission spectra in the solid state at RT and 77 K, complex **1** (left), complex **2** (middle) and complex **3** (right).

(exc. at 580 nm) and 662 nm (exc. at 500 nm) at room temperature, shifting the emissions at 1020 nm (exc. at 776 nm), 805 nm (exc. at 680 nm) and 768 nm (exc. at 550 nm) when the measurements were carried out at 77 K, respectively. The shift to lower energies of the emissions when the temperature decreases has been justified by a smaller HOMO–LUMO gap as a consequence of the shortening of the interatomic distances by thermal contractions at low temperature.[19]

In addition, the maxima of the excitation spectra of the three derivatives appear at lower energies to those of the corresponding diffuse reflectance spectra in the solid state. This could agree with the fact that these excitation bands are due to transitions in which metal centres are involved, which are forbidden transitions between triplet states. This is confirmed from the measurements of the lifetimes of the emissions for complexes **2** and **3** at room temperature (see Table 2), showing values in the range of microseconds, and therefore, are likely to be attributed to phosphorescence emissions.

Table 2 Photophysical properties of complexes **1–3**

Complex	**1**	**2**	**3**
Solid em (ex) (RT)	966 (550–694)	660 (280–580)	666 (280–500)
Solid em (ex) (77 K)	1020 (776)	805 (280–680)	768 (550)
τ (RT) μs	[a]	0.23	0.81
τ (77 K) μs	[a]	1.95	1.54
Φ (RT)	3.1	30.2	56.7

[a] Not affordable.

Interestingly, the emissions observed in these complexes appear near the limit of the visible range in the case of **2** or **3**, or even beyond in the case of **1**, at room temperature and at 77 K, which is a novel result considering those obtained in previous reports of gold–thallium derivatives with different ligands and with the same or different donor centres and geometries. Obviously, this fact can have its origin in the particular electronic characteristics of these terpyridine ligands that cause a shortening of the energy difference between the frontier orbitals, as can be seen by means of computational studies on the models of these derivatives.

Computational studies

Single point DFT calculations were performed to explain the origin of the emission of the complexes based on their solid-state structures. For this, we have built up tetranuclear model systems of complexes **1** and **2**, based on their crystal structures, representing all the interactions observed experimentally. We computed a model system of complex **1** $[Au_2Tl_2(C_6Cl_5)(\mathbf{L_1})_2]$ (model **1a**) to gain insight into the NIR emissive behaviour observed experimentally, and we computed a model system of complex **2** $[Au_2Tl_2(C_6Cl_5)(\mathbf{L_2})_2]$ (model **2a**) since it represents the similar visible emissions and lifetimes found experimentally for complexes **2** and **3**.

The first 30 singlet–singlet excitations were computed at the TD-DFT level of theory for the model systems of compounds **1–2** (see Tables 3 and 4). We also computed the lowest singlet–triplet excitation for both models in order to represent

Table 3 TD-DFT first singlet–singlet and lowest singlet–triplet excitation (Exc.) wavelengths ($\lambda_{calc.}$) and oscillator strengths (f) calculated for model **1a**

Model	Exc.	$\lambda_{calc.}$ (nm)	f	Contributions
1a	$S_0 \rightarrow T_1$	655	—	HOMO → LUMO (100%)
	$S_0 \rightarrow S_1$	635	0.0394	HOMO → LUMO (100%)
	$S_0 \rightarrow S_7$	431	0.2940	HOMO → LUMO+3 (57%)
	$S_0 \rightarrow S_{30}$	359	0.0642	HOMO−1 → LUMO+5 (32%)
				HOMO−1 → LUMO+3 (28%)

Table 4 TD-DFT first singlet–singlet and lowest singlet–triplet excitations (Exc.) wavelengths ($\lambda_{calc.}$) and oscillator strengths (f) calculated for model **2a**

Model	Exc.	$\lambda_{calc.}$ (nm)	f	Contributions
2a	$S_0 \rightarrow T_1$	510	—	HOMO → LUMO (84%)
	$S_0 \rightarrow S_1$	460	0.1374	HOMO → LUMO (97%)
	$S_0 \rightarrow S_{29}$	333	0.1128	HOMO → LUMO+5 (43%)
				HOMO → LUMO+7 (19%)
	$S_0 \rightarrow S_{30}$	332	0.0756	HOMO−14 → LUMO (68%)

the origin of their possible phosphorescent behaviour. The analysis of the most intense (in terms of oscillator strength) singlet–singlet transitions for model **1a** shows that they appear between 635 and 359 nm, the most intense excitation wavelengths appearing at 635, 431 and 359 nm.

In the case of the model system of model **2a** (representing the emissive properties of complexes **2** and **3**) TD-DFT calculations allow for the identification of the main transitions responsible for the spectral profile, the computed singlet–singlet excitations appear in a more energetic range than in model **1a** and also agree well with the more energetic experimental absorption profile obtained for these complexes. Thus, regarding model **2a**, the computed singlet–singlet transitions appear between 460 nm and 332 nm which are slightly overestimated.

As can be seen in Table 5, in the case of model **1a** the highest occupied molecular orbital (HOMO) displays a metal-based character (40% of gold contribution and 30% of thallium centres) with some contribution of the terpyridine $\mathbf{L_1}$, while the lowest unoccupied molecular orbital (LUMO) is mainly localized on the other terpyridine $\mathbf{L_1}$ ligand (95% of contribution). HOMO−1 shows a pentachlorophenyl ligand-based character (86%) with some contribution from Au(I) (11%). LUMO+3 and LUMO+5 exhibit terpyridine $\mathbf{L_1}$-based characters (67% and 69%, respectively) with minor metal (17% and 14%) and pentachlorophenyl contributions (18% in both cases).

Table 5 Selected frontier molecular orbital composition (%)

Model	Orbital	Au	Tl	C_6Cl_5	N-ligand
1a	LUMO+5	3	12	12	69
	LUMO+3	5	12	18	67
	LUMO	0	3	1	95
	HOMO	40	30	16	15
	HOMO−1	11	0	87	1
2a	LUMO+7	12	14	40	32
	LUMO+5	3	8	11	79
	LUMO	10	67	22	2
	HOMO	49	13	34	2
	HOMO−14	31	8	54	8

In the case of model **2a**, the HOMO shows a gold-based character (49%) with a pentachlorophenyl contribution (34%). HOMO−14 shows a pentachlorophenyl ligand-based character (54%) and a metal-based character (31% of Au(I) and 9% of Tl (I)). Meanwhile, unoccupied orbitals show the following characters: the LUMO exhibits a thallium-based character (67%) with a pentachlorophenyl contribution (22%); LUMO+3 exhibits mainly a terpyridine $\mathbf{L_2}$-character (79%) and LUMO+7 exhibits a ligand-based character with a contribution from pentachlorophenyl (40%) and terpyridine $\mathbf{L_2}$ (32%).

In view of the above, the assignment of the excitations is as follows: in model **1a**, the less energetic transitions appearing at 635 and 431 nm are attributed to metal (Au and Tl) to terpyridine $\mathbf{L_1}$ charge transfer transitions (^{1}MM′LCT), whereas the one at 359 nm is attributed to a pentachlorophenyl ligand to terpyridine $\mathbf{L_1}$ ligand charge transfer transition (LL′CT). The profile of the computed singlet–singlet excitations and TD-DFT calculations allow for the identification of the main transitions responsible for the spectral profile of complex **1**. In addition, the computed singlet–triplet transition at 655 nm matches the experimental excitation spectrum and consists of a metal (Au and Tl) to terpyridine $\mathbf{L_1}$ charge transfer transition (^{3}MM′LCT) that could be the origin of a possible phosphorescence behaviour of this complex.

In the case of model **2a** the intense singlet–singlet excitation at 460 nm consists of a transition involving both Au and Tl centres from a σ* MO to a σ bonding one. The excitation at 333 nm consists of a transition from the $[Au(C_6Cl_5)_2]^-$ fragment to the terpyridine $\mathbf{L_2}$ ligand. Finally, the transition of 332 nm can be assigned from the $[Au(C_6Cl_5)_2]^-$ fragment to the thallium centre. The calculated lowest singlet–triplet excitation at 510 nm also agrees well with the experimental excitation spectrum and consists of a transition involving both Au and Tl centres from a σ* MO to a σ bonding one (^{3}MM′) as responsible for the phosphorescence behaviour of complexes **2** and **3**.

In view of the computed excitations, it is likely that the emissive properties of complex **1** would arise from a forbidden metal-to-ligand charge transfer from the metals (Au and Tl) to terpyridine $\mathbf{L_1}$ (Fig. 7). Meanwhile, in the case of complexes **2** and **3**, the origin of the emissive behaviour is likely to be a for-

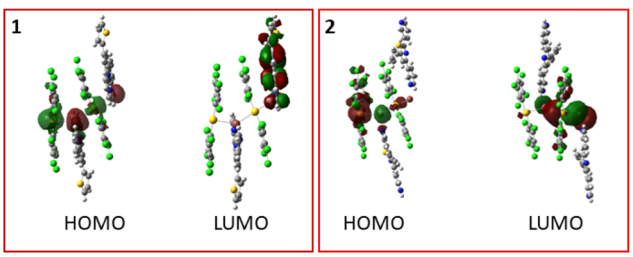

Fig. 7 Frontier molecular orbitals for models **1a** and **2a**.

bidden metal-centred transition along the heterometallic chain.

Conclusions

The synthesis of new heterometallic Au(I)/Tl(I) compounds *via* unsupported interactions has been investigated. In this case, the variation in the relative positions of the N-donor centres in three terpyridine-type ligands functionalized with the thiophene group has been analysed. This has allowed us to obtain two types of coordination modes. In the case of the ligand with N-donors at the *ortho* position, the ligand acts as a chelate, resulting in a one-dimensional polymeric chain, while for ligands with N-donors in the *meta* and *para* positions, it acts as a bridge between adjacent polymetallic chains, generating two-dimensional networks.

Regarding their optical properties, it has been observed that these compounds exhibit red-shifted emissions due to the terpyridine ligands. Additionally, the emissions observed in the solid state for compounds **2** and **3** are in the limit of the visible range, whereas for compound **1**, they appear in the infrared range, and this is the first time an Au–Tl compound shows this range of emission. Therefore, one of the most interesting results is the possibility of stretching the emission well into the NIR through the rational design of different complexes by the variation of the ligands' coordination sites, and the resulting difference in the coordination geometry and dimensionality of the compounds.

Through DFT calculations of tetranuclear models of compounds **1** and **2** based on their crystal structures, this behaviour has been understood. The emissive properties of complex **1** are likely to arise from a forbidden metal-to-ligand charge transfer from the metals (Au and Tl) to terpyridine $\mathbf{L_1}$. Meanwhile, in the case of complexes **2** and **3**, the origin of the emissive behaviour is likely to be a forbidden metal-centred transition along the heterometallic chain.

Therefore, combining the use of terpy ligands with their chelate bonding to thallium(I) centres (as observed for complex **1**), novel NIR emitters can be designed. Extrapolation of these conditions to other heterometallic systems to generalize this behaviour are under progress.

Experimental section

General

$AuTl(C_6Cl_5)_2$was prepared according to the literature.[14]

Materials and physical measurements

Infrared spectra were recorded in the 4000–450 cm^{-1} range on a PerkinElmer FT-IR Spectrum Two with a UATR (single reflection diamond) accessory. ^1H NMR spectra were recorded on a Bruker Avance 300 in dimethyl sulfoxide solutions. Chemical shifts have been quoted relative to $SiMe_4$ (^1H external). MALDI mass spectra were registered on a Microflex Bruker spectrometer using DCTB (T-2-(3-(4-*t*-butylphenyl)-2-methyl-2-propenylidene)-malononitrile) as the matrix. The *m*/*z* values are given for the higher peak in the isotopic pattern. Excitation and emission spectra in the solid state were recorded with an Edinburgh FLS 1000 fluorescence spectrometer. Luminescence lifetime was measured on an Edinburgh FLS 1000 fluorescence spectrometer. The equipment available in our laboratory did not allow us to measure lifetimes greater than 50 ns in the NIR range. Therefore, this measurement could not be carried out. For complex **1**, quantum yields were measured in the solid state using a Hamamatsu Quantaurus-QY C11347-11 integrating sphere. The low value obtained for complex **1** is due to the available range limit of measurement, up to *ca.* 900 nm, of the equipment used.

Synthesis

Synthesis of of $\mathbf{L_1}$, $\mathbf{L_2}$ and $\mathbf{L_3}$. The corresponding acetylpyridine (2.05 g, 0.017 mol) was added to a solution of the corresponding pyridine carboxylaldehyde (0.92 g, 0.009 mol) in ethanol (50 mL), and then granulated KOH (1.18 g, 0.021 mol) and NH_3 (25% solution in water, 4 mL) were added to the mixture. The reaction mixture was stirred at r.t. for 4 h. The resulting crystals were filtered off, washed with water, petroleum ether and recrystallized from a mixture of alcohol–$CHCl_3$. This procedure is a modified method.[20]

4′-(Thiophen-2-yl)-2,2′:6′,2″-terpyridine ($\mathbf{L_1}$). Yield 59% (5.11 g, 0.016 mol), white needles. m.p. = 185 °C. NMR ^1H (DMSO-d_6, 600.2 MHz): δ 8.79 (2H, br.dq, J = 1.0 and J = 4.0 Hz, H-6,6″-pyr), 8.67 (2H, br.s, H-3′,5′-pyr), 8.65 (2H, m, H-3,3″-pyr), 8.05 (2H, dt, J = 1.5 and J = 7.6 Hz, H-4,4″-pyr), 7.98 (1H, dd, J = 1.0 and J = 3.5 Hz, H-3-thienyl), 7.83 (1H, dd, J = 1.0 and J = 5.5 Hz, H-5-thienyl), 7.53 (2H, ddd, J = 1.5, J = 5.0 and J = 7.6 Hz, H-5,5″-pyr), 7.30 (1H, dd, J = 1.5, J = 4.0 and J = 5.0 Hz, H-4-thienyl) ppm. NMR ^{13}C ($CDCl_3$, 150.9 MHz): δ 156.2, 149.2, 143.5, 142.0, 136.9, 136.9, 128.4, 127.2, 125.9, 123.9, 121.4, 117.2 ppm. IR ν_{max}/cm^{-1} (KBr): 3050(m), 1598(s), 1580(s), 1565(m), 1545(m), 1463(w), 1445(m), 1265(w), 1121(m), 845(m), 769(m), 620(m). Elemental analysis calcd for $C_{19}H_{13}N_3S$: C, 72.36; H, 4.15; N, 13.32; found: C, 72.46; H, 4.01; N, 13.14.

4′-(Thiophen-2-yl)-3,2′:6′,3″-terpyridine ($\mathbf{L_2}$). Yield 62% (5.37 g, 0.017 mol), crystals. m.p. = 195–196 °C. NMR ^1H ($CDCl_3$, 600.2 MHz): δ 9.34 (2H, br.d, J = 2.2 Hz, H-2,2″-pyr), 8.69 (2H, br.dd, J = 1.5 and J = 4.4 Hz, H-6,6″-pyr), 8.46 (2H, br.td, J = 2.2 and J = 8.1 Hz, H-4,4″-pyr), 7.89 (2H, br.s, H-3′,5′-pyr), 7.63 (1H, br.dd, J = 1.5 and J = 3.7 Hz, H-3-thienyl), 7.47 (1H, m, H-5-thienyl), 7.45 (2H, m, H-5,5″-pyr), 7.19 (1H, m, H-4-thienyl) ppm. NMR ^{13}C ($CDCl_3$, 150.9 MHz): δ 155.6, 150.4, 148.5, 143.7, 141.1, 134.5, 128.7, 127.7, 125.9, 123.6, 115.9 ppm. IR ν_{max}/cm^{-1} IR ν_{max}/cm^{-1} (KBr): 3056(m), 1602(s), 1589(s), 1570(m), 1546(m), 1482(w), 1446(m), 1252(w), 1116(m), 837(m), 769(m), 654(m). Elemental analysis calcd for $C_{19}H_{13}N_3S$: C, 72.36; H, 4.15; N, 13.32; found: C, 72.43; H, 4.17; N, 13.16.

4′-(Thiophen-2-yl)-4,2′:6′,4″-terpyridine ($\mathbf{L_3}$). Yield 57% (4.93 g, 0.015 mol), crystals. m.p. = 242–243 °C. NMR ^1H (DMSO-D_6,

600.2 MHz): δ 8.78 (4H, br.d, J = 4.5 Hz, H-2,2″,6,6″-pyr), 8.38 (2H, br.s, H-3′,5′-pyr), 8.30 (4H, m, H-3, 3″,5,5″-pyr), 8.10 (1H, br.s, H-3-thienyl), 7.87 (1H, br.d, J = 5.0 Hz, H-5-thienyl), 7.31 (1H, m, H-4-thienyl) ppm. NMR ^{13}C ($CDCl_3$, 150.9 MHz): δ ppm. IR ν_{max}/cm^{-1} (KBr): 3025(m), 1591(s), 1558(s), 1537(m), 1494(m), 1421(w), 1402(m), 1259(w), 1063(m), 853(m), 769(m), 627(m). Elemental analysis calcd for $C_{19}H_{13}N_3S$: C, 72.36; H, 4.15; N, 13.32; found: C, 72.24; H, 4.38; N, 13.39.

*Synthesis of [AuTl(C$_6$Cl$_5$)$_2$(L$_1$)]$_n$ (**1**).* To a solution of [AuTl(C_6Cl_5)$_2$] (0.040 g, 0.044 mmol) in THF (30 mL) was added **L$_1$** (0.014 g, 0.044 mmol). The reaction mixture was stirred at room temperature for 15 min. Total evaporation of the solvent from the reaction mixture under vacuum and the addition of dichloromethane to the solid product resulted in the separation of a soluble part containing impurities and an insoluble solid corresponding to complex **1** as a black solid. Yield 60% (0.035 g). ^{1}H NMR (300 MHz, [D$_6$]-DMSO, 298 K), δ 8.81 (d,2H, H$_1$) [$^3J_{H1-H4}$ = 4 Hz], 8.74 (d,2H,H$_2$) [$^3J_{H2-H7}$ = 9 Hz], 8.71 (s,2H, H$_3$), 8.13 (pt,2H,H$_4$) [$^3J_{H1-H4}$–$^3J_{H4-H7}$ = 9 Hz], 8.05 (d,1H,H$_5$) [$^3J_{H5-H8}$ = 6 Hz], 7.85 (d,1H,H$_6$) [$^3J_{H6-H8}$ = 3 Hz], 7.62 (m,2H, H$_7$), 7.31 (pt,1H,H$_8$) [$^3J_{H8-H5}$–$^3J_{H8-H6}$ = 6 Hz] FT-IR: ν = 1600 cm^{-1} (C═N), ν = 1480 cm^{-1} (C═C), ν = 838 and 613 cm^{-1} (Au-C_6Cl_5). MALDI (+): m/z (%): 519 (100%) [Tl(L$_1$)]$^+$. MALDI (−): m/z (%): 694 (100%) [Au(C_6Cl_5)$_2$]$^-$. Λ_M (methanol): 115.2 Ω^{-1} cm^2 mol^{-1}.

*Synthesis of [{AuTl(C$_6$Cl$_5$)$_2$}$_2$(L$_2$)]$_n$ (**2**).* To a solution of [AuTl(C_6Cl_5)$_2$] (0.080 g, 0.088 mmol) in THF (30 mL) was added **L$_2$** (0.014 g, 0.044 mmol). The reaction mixture was stirred at room temperature for 15 min. Total evaporation of the solvent from the reaction mixture under vacuum and the addition of dichloromethane to the solid product resulted in the separation of a soluble part containing impurities and an insoluble solid corresponding to complex **2** as a red solid which emits red under a UV lamp. Yield 71% (0.067 g). ^{1}H NMR (300 MHz, [D$_6$]-DMSO, 298 K), δ 9.88 (s,2H,H$_1$), 9.55 (d,2H,H$_2$) [$^3J_{H2-H4}$ = 9 Hz], 9.06 (d,2H,H$_3$) [$^3J_{H3-H4}$ = 3 Hz], 8.62 (s,2H,H$_5$), 8.28 (pt,2H,H$_4$) [$^3J_{H4-H2}$–$^3J_{H4-H3}$ = 9 Hz], 8.21 [d,1H,H$_8$] [$^3J_{H8-H7}$ = 3 Hz], 7.92 [d,1H,H$_6$] [$^3J_{H6-H7}$ = 3 Hz], 7.35 (pt,1H,H$_7$) [$^3J_{H7-H8}$–$^3J_{H7-H6}$ = 3 Hz] FT-IR: ν = 1600 cm^{-1} (C═N), ν = 1423 cm^{-1} (C═C), ν = 838 and 616 cm^{-1} (Au–C_6Cl_5). MALDI (+): m/z (%): 705.06 (100%) [Tl(DCTB)$_2$]$^+$. MALDI (−): m/z (%): 694 (100%) [Au(C_6Cl_5)$_2$]. Λ_M (methanol): 70.8 Ω^{-1} cm^2 mol^{-1}.

*Synthesis of [AuTl(C$_6$Cl$_5$)$_2$(L$_3$)]$_n$ (**3**).* To a solution of [AuTl(C_6Cl_5)$_2$] (0.040 g, 0.044 mmol) in THF (30 mL) was added **L$_3$** (0.014 g, 0.044 mmol). The reaction mixture was stirred at room temperature for 15 min. Total evaporation of the solvent from the reaction mixture under vacuum and the addition of dichloromethane to the solid product resulted in the separation of a soluble part containing impurities and an insoluble solid corresponding to complex **3** as an orange solid which emits orange under a UV lamp. Yield 70% (0.037 g). ^{1}H NMR (300 MHz, [D$_6$]-DMSO, 298 K), δ 9.10 (d,4H,H$_1$) [$^3J_{H1-H2}$ = 6 Hz], 8.93(d,4H,H$_2$) [$^3J_{H1-H2}$ = 6 Hz], 8.74 (s,2H,H$_3$), 8.27 (d,1H, H6) [$^3J_{H6-H5}$ = 3 Hz], 7.94 (d,1H,H$_4$) [$^3J_{H4-H5}$ = 3 Hz], 7.38 (pt,1H,H$_5$) [$^3J_{H6-H5}$–$^3J_{H4-H5}$ = 6 Hz]. FT-IR: ν = 1593 cm^{-1} (C═N), ν = 1424 cm^{-1} (C═C), ν = 823 and 616 cm^{-1} (Au-C_6Cl_5). MALDI (+): m/z (%): 454 (100%) [Tl(DCTB)]$^+$. MALDI (−): m/z (%): 694 (100%) [Au(C_6Cl_5)$_2$]$^-$. Λ_M (methanol): 119.9 Ω^{-1} cm^2 mol^{-1}.

Crystallography

The crystal structures of complexes **1–3** were established by X-ray diffraction studies on single crystals grown by slow diffusion of *n*-hexane into a saturated solution of the complex in tetrahydrofuran (**1**) or acetone (**2** and **3**). Crystals were mounted in inert oil on a MiteGen MicroMountTM and transferred to the cold gas stream of a Bruker APEX-II CCD diffractometer equipped with an Oxford Instruments low-temperature attachment. Data were collected using monochromated Mo Kα radiation (λ = 0.71073 Å). Scan type: ω and ϕ. Absorption corrections: numerical (**1**) or empirical (**2** and **3**). The structures were solved with the XT structure solution program using intrinsic phasing and refined with the ShelXL refinement package using least squares minimization and refined on F^2 using the program SHELXL-2014/7.[21] One of the pentachlorophenyl rings in **1** and one of the thallium atoms in **2** are disordered over two different positions (65 : 35 and 65 : 35, respectively). All non-hydrogen atoms, except the carbon atoms of the disordered pentachlorophenyl group in **1**, were refined anisotropically. Hydrogen atoms were included using a riding model. CCDC 2305451–2305453 contain the supplementary crystallographic data for this paper.†

Computational details

All calculations were performed using the Gaussian 09 suite of programs[22] using the DFT-B3LYP level of theory.[23] The basis set combinations employed for the metals Au and Tl were the 19-VE and 21-VE pseudopotentials from Stuttgart and the corresponding basis sets were augmented with two *f* polarization functions.[24] The rest of the atoms were treated with SVP basis sets.[25] TD-DFT calculations were performed to compute the first 30 singlet–singlet excitations and the lowest singlet–triplet excitation for both models (**1a** and **2a**).

Conflicts of interest

There are no conflicts to declare.

Acknowledgements

We gratefully acknowledge PID2022-139739NB-l00 funded by MCIN/AEI/10.13039.

We are also grateful to the University of Maragheh for the financial support of this research. The publication has been prepared with the support from the "RUDN University Program 5-100" (recipient F. I. Zubkov, synthesis of the ligands).

References

1 See for example: (*a*) H. Schmidbaur and A. Schier, *Chem. Soc. Rev.*, 2008, **37**, 1931–1951; (*b*) H. Schmidbaur and A. Schier, *Chem. Soc. Rev.*, 2012, **41**, 370–412.

2 C. Silvestru and A. Laguna, in *The Chemistry of Organogold Compounds*, ed, Z. Rappoport, I. Marek, J. F. Liebman and S. Patai, Wiley, Chichester, UK, 2014, 409–526.

3 See for example: (*a*) *Gold Chemistry: Applications and Future Directions in the Life Sciences*, ed. F. Mohr, Wiley-VCH, Weinheim, Germany, 2009; (*b*) *Modern Supramolecular Gold Chemistry: Gold-Metal Interactions and Applications*, ed. A. Laguna, Wiley-VCH, Weinheim, Germany, 2008; (*c*) J. M. Forward, J. P. Fackler Jr. and Z. Assefa, Photophysical and Photochemical Properties of Gold(I) Complexes, in *Optoelectronic Properties of Inorganic Compounds*, ed. D. M. Roundhill and J. P. Fackler Jr., Springer, New York, 1999; (*d*) V. W.-W. Yam, V. K.-M. Au and S. Y.-L. Leung, *Chem. Rev.*, 2015, **115**, 7589–7728; (*e*) M. J. Katz, K. Sakai and D. B. Leznoff, *Chem. Soc. Rev.*, 2008, **37**, 1884–1895; (*f*) X. Hang, B. Li, Z.-H. Chen and Z.-N. Chen, *J. Mater. Chem.*, 2012, **22**, 11427–11441; (*g*) C. E. Strasser and V. J. Catalano, *J. Am. Chem. Soc.*, 2010, **132**, 1009–10011; (*h*) M. Ganguly, J. Jana, A. Pal and T. Pal, *RSC Adv.*, 2016, **6**, 17683–17703; (*i*) E. J. Fernández, A. Laguna and J. M. López-de-Luzuriaga, *Dalton Trans.*, 2007, 1969–1981; (*j*) J. M. López-de-Luzuriaga, M. Monge and M. E. Olmos, *Dalton Trans.*, 2017, **46**, 2046–2067; (*k*) R. J. Roberts, D. Le and D. B. Leznoff, *Chem. Commun.*, 2015, **51**, 14299–14302; (*l*) S. H. Lim, M. M. Olmstead and A. L. Balch, *J. Am. Chem. Soc.*, 2011, **133**, 10229–10238.

4 See for example: (*a*) M. E. Olmos, A. Schier and H. Schmidbaur, *Z. Naturforsch., B: Chem. Sci.*, 1997, **52**, 203–208; (*b*) E. J. Fernández, J. M. López-de-Luzuriaga, M. Monge, M. A. Rodríguez, O. Crespo, M. C. Gimeno, A. Laguna and P. G. Jones, *Chem. – Eur. J.*, 2000, **6**, 636–644; (*c*) I. O. Koshevoy, A. J. Karttunen, I. S. Kritchenkou, D. V. Krupenya, S. I. Selivanov, A. S. Melnikov, S. P. Tunik, M. Haukka and T. A. Pakkanen, *Inorg. Chem.*, 2013, **52**, 3663–3673; (*d*) V. J. Catalano and A. L. Moore, *Inorg. Chem.*, 2005, **44**, 6558–6566; (*e*) A. Laguna, T. Lasanta, J. M. López-de-Luzuriaga, M. Monge, P. Naumov and M. E. Olmos, *J. Am. Chem. Soc.*, 2010, **132**, 456–457; (*f*) E. Cerrada, M. Contel, A. D. Valencia, M. Laguna, T. Gelbrich and M. B. Hursthouse, *Angew. Chem., Int. Ed.*, 2000, **39**, 2353–2356; (*g*) I. O. Koshevoy, P. V. Ostrova, A. J. Karttunen, A. S. Melnikov, M. A. Khodorkovskiy, M. Haukka, J. Jänis, S. P. Tunik and T. A. Pakkanen, *Dalton Trans.*, 2010, **39**, 9022–9031; (*h*) Q.-M. Wang, Y.-A. Lee, O. Crespo, J. Deaton, C. Tang, H. J. Gysling, M. C. Gimeno, C. Larraz, M. D. Villacampa, A. Laguna and R. Eisenberg, *J. Am. Chem. Soc.*, 2004, **126**, 9488–9489; (*i*) J. R. Shakirova, E. V. Grachova, V. V. Gurzhiy, S. K. Thangaraj, J. Jänis, A. S. Melnikov, A. J. Karttunen, S. P. Tunik and I. O. Koshevoy, *Angew. Chem., Int. Ed.*, 2018, **57**, 14154–14158.

5 See for example: (*a*) K. Chen, C. E. Strasser, J. C. Schmitt, J. Shearer and V. J. Catalano, *Inorg. Chem.*, 2012, **51**, 1207–1209; (*b*) I. O. Koshevoy, J. R. Shakirova, A. S. Melnikov, M. Haukka, S. P. Tunik and T. A. Pakkanen, *Dalton Trans.*, 2011, **40**, 7927–7933; (*c*) M. J. Calhorda, C. Ceamanos, O. Crespo, M. C. Gimeno, A. Laguna, C. Larraz, P. D. Vaz and M. D. Villacampa, *Inorg. Chem.*, 2010, **49**, 8255–8269; (*d*) I. O. Koshevoy, Y.-C. Chang, A. J. Karttunen, M. Haukka, T. Pakkanen and P.-T. Chou, *J. Am. Chem. Soc.*, 2012, **134**, 6564–6567; (*e*) G. F. Manbeck, W. W. Brennessel, R. A. Stockland Jr. and R. Eisenberg, *J. Am. Chem. Soc.*, 2010, **132**, 12307–12318; (*f*) I. O. Koshevoy, C.-L. Lin, A. J. Karttunen, J. Jänis, M. Haukka, S. P. Tunik, P.-T. Chou and T. A. Pakkanen, *Chem. – Eur. J.*, 2011, **17**, 11456–11466; (*g*) D. V. Krupenya, P. A. Snegurov, E. V. Grachova, V. V. Gruzhiy, S. P. Tunik, A. S. Melnikov, P. Y. Serdobintsev, E. G. Vlakh, E. S. Sinitsyna and T. B. Tennikova, *Inorg. Chem.*, 2013, **52**, 12521–12528; (*h*) J. R. Shakirova, E. V. Grachova, V. V. Gurzhiy, I. O. Koshevoy, A. S. Melnikov, O. V. Sizova, S. P. Tunik and A. Laguna, *Dalton Trans.*, 2012, **41**, 2941–2949; (*i*) I. O. Koshevoy, A. J. Karttunen, S. P. Tunik, M. Haukka, S. I. Selivanov, A. S. Melnikov, P. Y. Serdobintsev, M. A. Khodorkovskiy and T. A. Pakkanen, *Inorg. Chem.*, 2008, **47**, 9478–9488; (*j*) I. O. Koshevoy, A. J. Karttunen, S. P. Tunik, J. Jänis, M. Haukka, A. S. Melnikov, P. Y. Serdobintsev and T. A. Pakkanen, *Dalton Trans.*, 2010, **39**, 2676–2683; (*k*) A. Belyaev, T. Eskelinen, T. M. Dau, Y. Y. Ershova, S. P. Tunik, A. S. Melnikov, P. Hirva and I. O. Koshevoy, *Chem. – Eur. J.*, 2018, **24**, 1404–1415; (*l*) M. M. Nenzel, K. Chen and V. J. Catalano, *J. Coord. Chem.*, 2016, **69**, 160–167; (*m*) K. Chen and V. J. Catalano, *Eur. J. Inorg. Chem.*, 2015, 5254–5261.

6 See for example: (*a*) R. Echeverría, J. M. López-de-Luzuriaga, M. Monge and M. E. Olmos, *Chem. Sci.*, 2015, **6**, 2022–2026; (*b*) R. Echeverría, J. M. López-de-Luzuriaga, M. Monge, S. Moreno and M. E. Olmos, *Inorg. Chem.*, 2016, **55**, 10523–10534; (*c*) R. Echeverría, J. M. López-de-Luzuriaga, M. Monge, S. Moreno, M. E. Olmos and M. Rodríguez-Castillo, *Chem. Commun.*, 2018, **54**, 295–298.

7 See for example: (*a*) S. Wang, J. P. Fackler Jr., C. King and J. C. Wang, *J. Am. Chem. Soc.*, 1988, **110**, 3308–3310; (*b*) S. Wang, G. Garzón, C. King, J.-C. Wang and J. P. Fackler Jr., *Inorg. Chem.*, 1989, **28**, 4623–4629; (*c*) V. J. Catalano, B. L. Bennett, H. M. Kar and B. C. Noll, *J. Am. Chem. Soc.*, 1999, **121**, 10235–10236.

8 E. J. Fernández, J. M. López-de-Luzuriaga, M. Monge, M. Montiel, M. E. Olmos and M. Rodríguez-Castillo, *Dalton Trans.*, 2009, **36**, 7509–7518.

9 J. M. López-de-Luzuriaga, G. Mahmoudi, M. Monge, M. E. Olmos, M. Rodríguez-Castillo, M. Villar, F. I. Zubkov and E. A. Kvyatkovskaya, *Inorg. Chem.*, 2020, **59**, 9443–9451.

10 E. J. Fernández, P. G. Jones, A. Laguna, J. M. López-de-Luzuriaga, M. Monge, J. Pérez and M. E. Olmos, *Inorg. Chem.*, 2002, **41**, 1056–1063.

11 E. J. Fernández, A. Laguna, J. M. López-de-Luzuriaga, M. Monge, M. Montiel and M. E. Olmos, *Inorg. Chem.*, 2007, **46**, 2953–2955.
12 O. Crespo, E. J. Fernández, P. G. Jones, A. Laguna, J. M. López-de-Luzuriaga, A. Mendía, M. Monge and M. E. Olmos, *Chem. Commun.*, 1998, **20**, 2233–2234.
13 E. J. Fernández, A. Laguna, J. M. López-de-Luzuriaga, M. E. Olmos and J. Pérez, *Dalton Trans.*, 2004, **12**, 1801–1806.
14 E. J. Fernández, J. M. López-de-Luzuriaga, M. Monge, M. E. Olmos, J. Pérez, A. Laguna, A. A. Mohamed and J. P. Fackler Jr., *J. Am. Chem. Soc.*, 2003, **125**, 2022–2023.
15 See for example: (*a*) A. J. Blake, R. Donamaría, E. J. Fernández, T. Lasanta, V. Lippolis, J. M. López-de-Luzuriaga, E. Manso, M. Monge and M. E. Olmos, *Dalton Trans.*, 2013, **42**, 11559–11570; (*b*) A. J. Blake, R. Donamaría, V. Lippolis, J. M. López-de-Luzuriaga, E. Manso, M. Monge and M. E. Olmos, *Inorg. Chem.*, 2014, **53**, 10471–10484; (*c*) R. Donamaría, M. C. Gimeno, V. Lippolis, J. M. López-de-Luzuriaga, M. Monge and M. E. Olmos, *Inorg. Chem.*, 2016, **55**, 11299–11310; (*d*) A. J. Blake, R. Donamaría, V. Lippolis, J. M. López-de-Luzuriaga, M. Monge, M. E. Olmos, A. Seal and J. A. Weinstein, *Inorg. Chem.*, 2019, **58**, 4954–4961; (*e*) R. Donamaría, V. Lippolis, J. M. López-de-Luzuriaga, M. Monge, M. Nieddu and M. E. Olmos, *Inorg. Chem.*, 2017, **56**, 12551–12563; (*f*) R. Donamaría, V. Lippolis, J. M. López-de-Luzuriaga, M. Monge, M. Nieddu and M. E. Olmos, *Chem. – Eur. J.*, 2018, **24**, 13740–13743; (*g*) R. Donamaría, V. Lippolis, J. M. López-de-Luzuriaga, M. Monge, M. Nieddu and M. E. Olmos, *Inorg. Chem.*, 2018, **57**, 11099–11111; (*h*) R. Donamaría, V. Lippolis, J. M. López-de-Luzuriaga, M. Monge, M. Nieddu and M. E. Olmos, *Inorg. Chem.*, 2020, **59**, 6398–6409.
16 E. J. Fernández, J. M. López-de-Luzuriaga, M. M. Monge, M. E. Olmos and J. Perez, *J. Am. Chem. Soc.*, 2003, **125**, 2022–2023.
17 R. Usón, A. Laguna, M. Laguna, B. R. Manzano and A. Tapia, *Inorg. Chim. Acta*, 1985, **101**, 151–153.
18 See for example: (*a*) E. J. Fernández, P. G. Jones, A. Laguna, J. M. López-de-Luzuriaga, M. Monge, M. Montiel, M. E. Olmos and J. Pérez, *Z. Naturforsch., B: Chem. Sci.*, 2004, **59**, 1379–1386; (*b*) M. Arca, R. Donamaria, M. C. Gimeno, V. Lippolis, J. M. López-de-Luzuriaga, E. Manso, M. Monge and M. E. Olmos, *Dalton Trans.*, 2015, **44**, 6719–6730; (*c*) E. J. Fernández, J. M. López-de-Luzuriaga, M. E. Olmos, J. Pérez, A. Laguna and M. C. Lagunas, *Inorg. Chem.*, 2005, **44**, 6012–6018.
19 S. Wang, G. Garzón, C. King, J. Wang and J. P. Fackler Jr., *Inorg. Chem.*, 1989, **28**, 4623–4629.
20 C. B. Smith, C. L. Raston and A. N. Sobolev, *Green Chem.*, 2005, **7**, 650–665.
21 G. M. Sheldrick, *SHELXL-2014/7, Program for Crystal Structure Refinement*, University of Göttingen, Germany, 2014.
22 M. J. Frisch, G. W. Trucks, H. B. Schlegel, G. E. Scuseria, M. A. Robb, J. R. Cheeseman, G. Scalmani, V. Barone, G. A. Petersson, H. Nakatsuji, X. Li, M. Caricato, A. Marenich, J. Bloino, B. G. Janesko, R. Gomperts, B. Mennucci, H. P. Hratchian, J. V. Ortiz, A. F. Izmaylov, J. L. Sonnenberg, D. Williams-Young, F. Ding, F. Lipparini, F. Egidi, J. Goings, B. Peng, A. Petrone, T. Henderson, D. Ranasinghe, V. G. Zakrzewski, J. Gao, N. Rega, G. Zheng, W. Liang, M. Hada, M. Ehara, K. Toyota, R. Fukuda, J. Hasegawa, M. Ishida, T. Nakajima, Y. Honda, O. Kitao, H. Nakai, T. Vreven, K. Throssell, J. A. Montgomery Jr., J. E. Peralta, F. Ogliaro, M. Bearpark, J. J. Heyd, E. Brothers, K. N. Kudin, V. N. Staroverov, T. Keith, R. Kobayashi, J. Normand, K. Raghavachari, A. Rendell, J. C. Burant, S. S. Iyengar, J. Tomasi, M. Cossi, J. M. Millam, M. Klene, C. Adamo, R. Cammi, J. W. Ochterski, R. L. Martin, K. Morokuma, O. Farkas, J. B. Foresman and D. J. Fox, *Gaussian 09, Revision A.1*, Gaussian, Inc., Wallingford CT, 2009.
23 A. D. Becke, *J. Chem. Phys.*, 1993, **98**, 5648–5652.
24 D. Andrae, U. Haeussermann, M. Dolg, H. Stoll and H. Preuss, Energy-adjusted ab initio pseudopotentials for the second and third row transition elements, *Theor. Chim. Acta*, 1990, **77**, 123–141.
25 A. Schäfer, H. Horn and R. J. Ahlrichs, *Chem. Phys.*, 1992, **97**, 2571–2577.